

Cognitive Chunking for Soft Prompts: Accelerating Compressor Learning via Block-wise Causal Masking

Guojie Liu*
 Yiqi Wang*
 liuguojie@nudt.edu.cn
 yiq@nudt.edu.cn
 National University of Defense
 Technology
 Changsha, China

Songlei Jian
 National University of Defense
 Technology
 Changsha, China
 jiansonglei@nudt.edu.cn

Yanfeng Yang
 National University of Defense
 Technology
 Changsha, China
 yanfengyang@nudt.edu.cn

Jianfeng Zhang
 National University of Defense
 Technology
 Changsha, China
 jfzhang@nudt.edu.cn

Wenqi Fan
 The Hong Kong Polytechnic
 University
 Hong Kong SAR, China
 wenqifan03@gmail.com

Jie Yu
 National University of Defense
 Technology
 Changsha, China
 yj@nudt.edu.cn

Abstract

Providing extensive context via prompting is vital for leveraging the capabilities of Large Language Models (LLMs). However, lengthy contexts significantly increase inference latency, as the computational cost of self-attention grows quadratically with sequence length. To mitigate this issue, context compression—particularly soft prompt compression—has emerged as a widely studied solution, which converts long contexts into shorter memory embeddings via a trained compressor. Existing methods typically compress the entire context indiscriminately into a set of memory tokens, requiring the compressor to capture global dependencies and necessitating extensive pre-training data to learn effective patterns. Inspired by the chunking mechanism in human working memory and empirical observations of the spatial specialization of memory embeddings relative to original tokens, we propose Parallelized Iterative Compression (PIC). By simply modifying the Transformer’s attention mask, PIC explicitly restricts the receptive field of memory tokens to sequential local chunks, thereby lowering the difficulty of compressor training. Experiments across multiple downstream tasks demonstrate that PIC consistently outperforms competitive baselines, with superiority being particularly pronounced in high compression scenarios (e.g., achieving relative improvements of 29.8% in F1 score and 40.7% in EM score on QA tasks at the 64 \times compression ratio). Furthermore, PIC significantly expedites the training process. Specifically, when training the 16 \times compressor, it surpasses the peak performance of the competitive baseline while effectively reducing the training time by approximately 40%.

Keywords

Context Compression, Large Language Models, Soft Prompt, Memory Embeddings

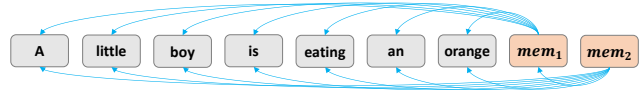


Figure 1: An illustration of unconstrained global attention in a typical soft prompt compression method: both memory tokens need to attend to all the input words simultaneously.

1 Introduction

To enhance the generation quality of Large Language Models (LLMs), incorporating extensive contextual information has become a common practice, providing essential background and task-specific clues in paradigms such as Retrieval-Augmented Generation (RAG) [10] and In-Context Learning (ICL) [17]. However, the extension of context length inevitably introduces significant computational overhead, leading to a substantial increase in inference latency and posing critical challenges for real-time applications.

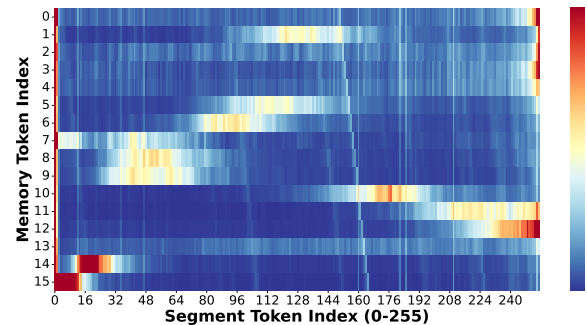
A promising direction to mitigate these issues is context compression, which aims to reduce the effective length of the input sequence while preserving its informational core. Existing compression approaches can be broadly categorized into two types: hard prompt compression and soft prompt compression [19]. Hard prompt compression typically relies on heuristic rules to prune redundant tokens from the original context or employs another LLM to produce a discrete, natural language summary, fundamentally retaining a symbolic representation [6, 13, 14, 18, 22]. In contrast, soft prompt compression learns a compact, continuous representation by distilling the context information into a small set of dense embedding vectors [4, 5, 9, 11, 20, 25], which can be viewed as a novel modality offering the potential for higher compression rates [9]. Therefore, this work focuses on soft prompt compression. Typically, the input context is processed by a compressor to yield a shortened sequence of continuous memory embeddings. These compressed representations—often further aligned in dimension and semantics via a converter layer—then replace the original context as input to the downstream decoder for generation.

*Both authors contributed equally to this research.

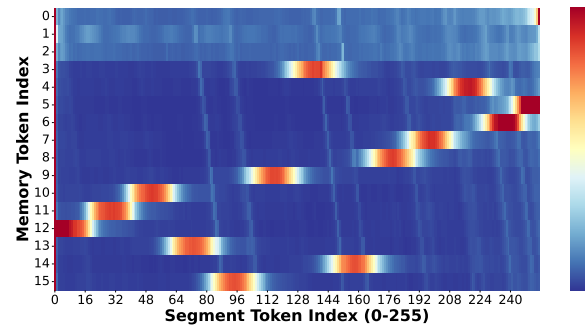
However, the majority of existing methods typically follow the described pipeline yet rely on unconstrained global attention to map the entire context into the fixed memory slots, as shown in Figure 1. In this design, the compressor lacks an inductive bias to establish explicit correspondences between specific memory tokens and particular input subsequences. As a result, each memory token typically needs to attend to and extract information from all tokens in the lengthy context [27], which encourages the model to implicitly learn complex global routing patterns. This process often increases the learning difficulty, tending to render the training process more data-intensive and time-consuming. [12]

The core challenge, therefore, lies in how the compressor allocates its limited memory tokens to retain essential information. To demystify the learned allocation strategy, we examine the interaction between memory tokens and original context tokens using a representative framework [9]. We compute both the attention weights and the cosine similarity between their corresponding embeddings on the HotpotQA dataset. The resulting heatmaps in Figure 2 (attention) and Figure 3 (embedding similarity) reveal a highly consistent and crucial evolution. As shown in Figure 2a, early in training (1k steps), attention from memory tokens to the input is diffuse and unstructured. However, after full convergence (90k steps), a clear block-wise pattern emerges (Figure 2b), where each memory token aligns strongly with a specific, contiguous segment of the context. This spatial specialization is not an artifact of the attention mechanism alone; it is directly corroborated by the embedding similarities in Figure 3, which exhibit an identical block-wise structure. This spatial specialization suggests that an desired strategy for maximizing information retention under the memory bottleneck is to partition the context and dedicate individual memory tokens to distinct blocks.

This observed correspondence, where memory tokens become selectively attuned to contiguous segments of the input context, bears a notable resemblance to the cognitive principle of chunking in human working memory [1, 2]. It is evident from cognitive studies that working memory, constrained by a limited capacity [8], compensates by organizing information into coherent, higher-order units or "chunks"—such as grouping digits in a phone number or phrases in a sentence—thereby facilitating efficient storage and recall [29]. However, a critical distinction exists: human comprehension unfolds sequentially, with each new segment being interpreted in light of previously integrated information. In contrast, existing compressors acquire this partitioning strategy implicitly, without enforcing a strict sequential correspondence between memory tokens and text blocks. This observation motivates us to explicitly impose a sequential, block-wise alignment, guiding each memory token to attend to a specific, ordered segment of the context. By doing so, we simplify the learning objective from global dependency modeling to localized information extraction, which has the potential to substantially reducing optimization complexity. To preserve the efficiency of parallel computation while maintaining sequential integrity, we further introduce a Parallelized Iterative Compression (PIC) approach. It employs a block-wise causal mask that simulates incremental, block-by-block processing in a single forward pass, thereby preserving order constraints without incurring the latency of sequential iteration.



(a) Compressor Trained for 1k Steps



(b) Fully Trained Compressor (90k Steps)

Figure 2: Attention weight heatmap between memory tokens and original context tokens. Red indicates higher attention weight, while blue represents lower attention weight.

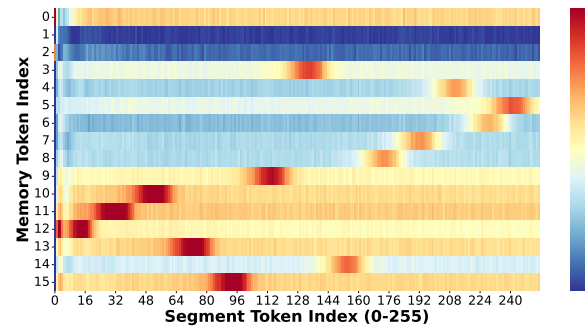


Figure 3: Heatmap visualization of the cosine similarity between generated memory embeddings generated by the fully trained compressor (90k steps) and the embeddings of original context tokens on the HotpotQA dataset. Red indicates higher similarity, while blue represents lower similarity.

Experiments on two representative downstream tasks—namely Retrieval-Augmented Generation (RAG) based Question Answering and In-Context Learning (ICL)—demonstrate that our method consistently outperforms competitive baselines, with the performance gap widening as the compression ratio increases. While achieving competitive results at low compression rates, our approach exhibits significantly stronger robustness when the memory budget becomes severely constrained (e.g., under 16 \times and 64 \times compression), confirming its superior efficiency in preserving task-relevant

information. To further verify that our design effectively reduces learning difficulty, we conduct a data-efficiency analysis. The results show that our method is substantially more data-efficient; specifically, under the $16\times$ compression setting, it enables the model to surpass the peak performance of baselines with approximately 40% less training time. The key contributions of this paper are summarized as follows:

- Through a systematic investigation of the interaction between memory embeddings and input context, we identify a clear spatial-specialization phenomenon that closely mirrors the cognitive chunking mechanism in human working memory.
- We propose an iterative compression method that explicitly restricts each memory token to attend only to a sequential block of the input context, thereby simplifying global modeling into local extraction.
- To enable efficient parallel execution while preserving sequential logic, we introduce Parallelized Iterative Compression (PIC), which approximates incremental block-wise processing via a novel block-wise causal mask.
- Extensive experiments demonstrate that our method not only accelerates compressor convergence but also achieves superior performance across multiple downstream tasks. Visualization studies further confirm that our approach successfully enforces the intended sequential block-to-token alignment and yields more orthogonal representations across different memory tokens.

2 Related Work

Existing context compression approaches fall into two broad categories: hard prompt compression and soft prompt compression [19]. Hard prompt compression, such as LLMLingua2 [22], produces compressed outputs in human-readable natural language, often by formulating the task as token-level classification. Our work focuses on soft prompt compression, which condenses text into continuous memory representations. Early methods like AutoCompressor [5] introduced iterative summary generation, while PPC [21] demonstrated that simple attention masks could guide models to compress prompts into “gist tokens.” Some follow-up works, such as xRAG [4], employ knowledge distillation as their primary training strategy, focusing on training only the modality bridge. Other frameworks, including ICAE [11], present a general compressor-decoder architecture pre-trained via reconstruction and prediction tasks. COCOM [25] further emphasizes that the downstream decoder requires additional fine-tuning to effectively utilize compressed memory. Subsequent analyses, such as PISCO [20], examine embedding behaviors in such settings. Building on these, PCC [9] explores fundamental design questions like scalability across compression ratios.

3 Method

Standard global compression approaches, which process the context indiscriminately, impose a heavy burden on the compressor to implicitly learn complex attention patterns. Motivated by the spatial specialization observed and the sequential nature of human reading, we introduce a sequential block-wise paradigm as the foundational logic for effective compression. This paradigm explicitly

mandates that context is compressed into memory slots through structured sequential segments to reduce optimization difficulty. Although a direct iterative implementation of this logic ensures structural integrity, it suffers from high latency. To resolve this trade-off between structure and efficiency, we propose Parallelized Iterative Compression (PIC). By leveraging a block-wise causal mask, PIC approximates the sequential iterative process in a fully parallelized manner. This design effectively retains the inductive bias of sequential processing while achieving the inference speed characteristic of direct global compression.

3.1 Problem Definition

The objective of soft prompt compression is to distill an input context $\mathbf{X} = (x_1, \dots, x_L)$ of L tokens into a compact memory representation $\tilde{\mathbf{H}} = (h_1, \dots, h_N)$, which is a concatenation of N embedding vectors, $N \ll L$ and L is divisible by N . These compressed embeddings subsequently replace the original context \mathbf{X} to facilitate downstream text generation tasks in an LLM:

$$f_{\text{LLM}}(\tilde{\mathbf{H}}, \text{prompt}) \rightarrow \mathbf{Y}_{\text{output}} \quad (1)$$

Most of the existent compression methods, as illustrated in Figure 4(a), formulate compression as a global mapping problem [9]. By introducing a set of N learnable memory tokens $\mathbf{M} = (m_1, \dots, m_N)$ as placeholders, the compressor processes the context \mathbf{X} along with these memory tokens to obtain the hidden states from the final layer as the memory embeddings $\tilde{\mathbf{H}}$. Therefore, the generation of each memory embedding h_t depends on the entire input context \mathbf{X} and the preceding memory tokens $m_{<t}$:

$$h_t = \text{Compressor}(\mathbf{X}, m_{<t}) \quad (2)$$

However, this direct compression approach can necessitate learning complex attention patterns and is typically sub-optimal.

3.2 Iterative Compression

To mitigate the difficulty of learning global dependencies, we draw inspiration from the limit capacity of human working memory and adopt an iterative compression strategy. As visually depicted in Figure 4, human working memory employs a chunking mechanism to organize continuous streams of information into discrete, manageable units for efficient processing. Mimicking this mechanism as shown in Figure 4(b), we decompose the input \mathbf{X} into N equal-length non-overlapping chunks $\mathbf{X} = (c_1, c_2, \dots, c_N)$. The compression process is then structured sequentially, where the t -th memory embedding h_t is generated by compressing only its corresponding chunk c_t , while maintaining access to the historical compressed memory $h_{<t}$. Accordingly, the generation process is reformulated as:

$$h_t = \text{Compressor}(c_t, h_{<t}) \quad (3)$$

This formulation introduces a structural inductive bias, enforcing a one-to-one mapping between memory tokens and context chunks. Consequently, the generation of h_t becomes local to the original text (attending only to c_t) but global to the compressed memory history ($h_{<t}$).

While iterative decomposition effectively simplifies global modeling by breaking it down into manageable local tasks, thereby

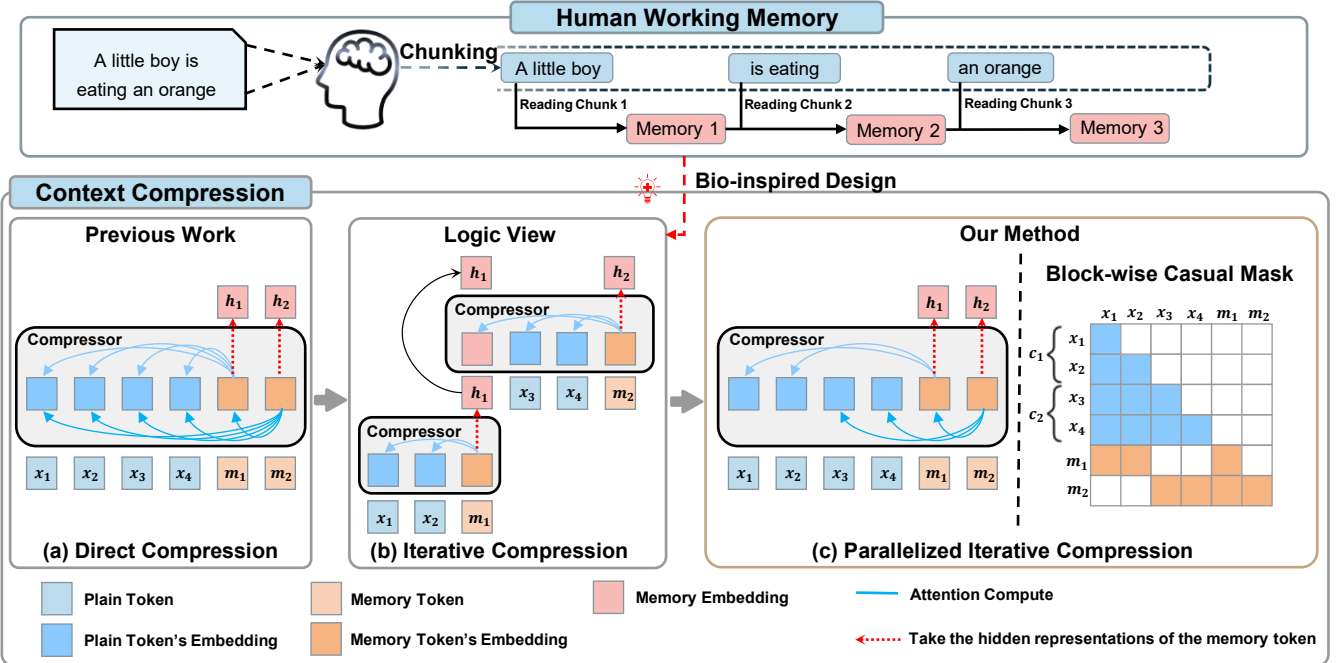


Figure 4: Comparison of different compression paradigms. (a) Direct Compression: Each memory token attends globally to the entire input context without structural constraints. (b) Iterative Compression: Inspired by the chunking mechanism in human working memory, we split the input context into chunks, and memory tokens are generated sequentially, with each token attending only to its specific chunk and previous memory. (c) Parallelized Iterative Compression (PIC): Our proposed method allows all memory tokens to be processed in parallel within a single sequence, using a block-wise causal mask to enforce the same local dependency constraints as the iterative approach.

alleviating the training burden, its strict sequential processing dependency inherently prohibits parallel computation. As a consequence, inference latency increases linearly with the number of memory tokens, creating a fundamental trade-off between optimization tractability and computational efficiency.

3.3 Parallelized Iterative Compression

To resolve the latency bottleneck of iterative compression while preserving its beneficial learning properties, we propose Parallelized Iterative Compression (PIC). As illustrated in Figure 4(c), PIC processes all context chunks and memory tokens simultaneously in a single forward pass. Crucially, it employs a block-wise causal attention mask to strictly simulate the receptive field of the sequential iterative process. This design allows the model to learn the simplified local objectives of iterative compression without incurring the latency of serial execution.

3.3.1 Sequence Construction. Unlike serial iterative methods that process chunks step-by-step, PIC concatenates all chunks and memory tokens into a single sequence for parallel processing. Let X be uniformly divided into N chunks $X = (c_1, c_2, \dots, c_N)$, and $\tilde{M} = (m_1, \dots, m_N)$ be the appended memory placeholders. The input sequence Z is constructed as:

$$Z = [c_1, c_2, \dots, c_N, m_1, m_2, \dots, m_N] = [X, \tilde{M}] \quad (4)$$

3.3.2 Block-wise Causal Attention Mask. Our core innovation is the block-wise causal attention mask, which enforces the iterative inductive bias within a single parallel pass. We design the mask $M \in \mathbb{R}^{|Z| \times |Z|}$ to ensure that each memory token m_t attends exclusively to its assigned chunk c_t and the memory history $m_{<t}$.

Let z_i, z_j be the query and key tokens in Z . We define a binary visibility indicator function $\text{Visible}(i, j) \in \{0, 1\}$, where 1 denotes that z_i is allowed to attend to z_j , according to three rules:

- (1) **Intra-Context Causal:** For tokens within the context ($z_i, z_j \in X$), $\text{Visible}(i, j) = 1$ if $i \geq j$.
- (2) **Intra-Memory Causal:** For tokens within the memory ($z_i, z_j \in \tilde{M}$), $\text{Visible}(i, j) = 1$ if $i \geq j$.
- (3) **Memory-to-Block Attention:** If the query is a memory token ($z_i \in \tilde{M}$ at index t) and the key is a context token ($z_j \in X$ belonging to chunk c_k), $\text{Visible}(i, j) = 1$ if $t = k$.

Formally, the mask entry $M_{i,j}$ is:

$$M_{i,j} = \begin{cases} 0 & \text{if } \text{Visible}(i, j) \\ -\infty & \text{otherwise} \end{cases} \quad (5)$$

This design effectively prevents m_t from accessing past chunks $c_{<t}$ directly, forcing the compressor to rely on the memory history $m_{<t}$ for context coherence. By compressing locally and connecting globally, PIC achieves logical equivalence to iterative compression without the serial latency.

Table 1: Basic Statistics of Data Samples for Datasets

Stage	Source	Train	Test
Pre-training	FineWeb	11,520,000	576
Fine-tuning(RAG)	SQuAD	86,821	5,928
Fine-tuning(ICL)	GSM8K	6,725	748

3.4 Pre-training and Fine-tuning

To ensure a fair comparison and rigorously validate the effectiveness of our block-wise causal mask, we align our training pipeline with the established PCC framework [9], utilizing identical pre-training tasks and fine-tuning objectives.

3.4.1 Pre-training Objectives. Text Reconstruction (TR). This task requires the model to reconstruct the original context X autoregressively, conditioned on the compressed memory \tilde{H} . A special token $\langle AE \rangle$ is appended to \tilde{H} to indicate the reconstruction task. The objective is formalized as:

$$\mathcal{L}_{TR} = -\frac{1}{L} \sum_{i=1}^L \log f_{LLM}(x_i \mid \tilde{H}, \langle AE \rangle, x_{<i}) \quad (6)$$

where $x_{<i}$ denotes the prefix sequence (x_1, \dots, x_{i-1}) .

Text Completion (TC). This objective encourages the memory representation to capture semantic information essential for future generation. We partition the text into a prefix and a continuation, where the memory \tilde{H} is compressed from the prefix. The model then predicts the continuation sequence starting from index $k+1$:

$$\mathcal{L}_{TC} = -\frac{1}{L-k} \sum_{i=k+1}^L \log f_{LLM}(x_i \mid \tilde{H}, x_k, \dots, x_{i-1}) \quad (7)$$

The total pre-training loss is a weighted sum of both objectives, with $\lambda = 0.5$:

$$\mathcal{L} = \lambda \mathcal{L}_{TC} + (1 - \lambda) \mathcal{L}_{TR} \quad (8)$$

3.4.2 Fine-tuning. For downstream adaptation, we conduct domain-specific fine-tuning. Following the experimental settings in PCC, we utilize a single representative dataset per task category to adapt the compressor.

4 Experiments

4.1 Experimental Setup

4.1.1 Datasets. Table 1 provides a summary of the datasets utilized across different training stages. In the pre-training stage, we leveraged approximately 3 billion tokens from the FineWeb [23] dataset. For the fine-tuning stage, two datasets were incorporated: SQuAD [24], comprising 86,821 training samples and 5,928 test samples, and GSM8K [7], containing 6,725 training samples and 748 test samples. Specifically, We employed the training set of SQuAD as the domain-specific dataset for the RAG-based Question Answering (QA) task, and GSM8K for the In-Context Learning (ICL) task.

4.1.2 Implementation Details. Our experiments primarily focus on efficient context compression using accessible model scales. During the pre-training phase, we explored architectures from two different

model families as compressors. Primarily, we engaged Qwen2.5-0.5B-Instruct as the compressor, trained via full-parameter fine-tuning, while the downstream decoder was Llama-3-8B-Instruct, which remained frozen. To eliminate potential biases arising from model family differences, we additionally trained a compressor based on Llama-3.2-1B-Instruct, also using full-parameter fine-tuning. In the pre-training stage, the learning rate was set to 1×10^{-4} for all models. Training the PIC model (with the Qwen backbone) for one full epoch on the pre-training dataset took approximately 170 hours on a single node with two 48GB RTX 4090 GPUs. For all inference experiments, greedy decoding was applied to the LLM decoder.

4.1.3 Baselines. We compare our approach against six competitive context compression methods:

AutoCompressor [5]: Adapts a pre-trained Llama-2-7b-hf to generate summaries embeddings, achieving a high compression ratio of 40x.

xRAG [4]: Utilizes Mistral-7B-Instruct-v0.2 as the downstream LLM. It focuses on training the connector (Convert module) while keeping other components frozen, fine-tuned on multiple downstream datasets.

COCOM [25]: Employs a compressor based on bert-base-uncased for pre-training and fine-tunes the downstream LLM (Mistral-7B-Instruct-v0.2).

ICAE [11]: Features a compressor pre-trained on Mistral-7B to compress context into memory slots, utilizing Mistral-7B-Instruct-v0.2 as the downstream LLM.

LLMLingua-2 [22]: A hard prompt compression method based on token classification (using XLM-RoBERTa-large). It is evaluated with Llama-3-8B-Instruct as the target LLM.

PCC [9]: The primary baseline. PCC-Lite utilizes a compressor pre-trained on GPT2-Large, while PCC-Large employs Llama-3-8B-Instruct. Both variants use Llama-3-8B-Instruct as the downstream decoder.

To ensure a fair comparison, we strictly adhered to the experimental settings established in PCC and directly compared our results against the metrics reported in their paper.

4.2 Main Results

4.2.1 RAG-based Question Answering. We first evaluate our compressor in the Retrieval-Augmented Generation (RAG) based Question Answering scenario. Each data sample consists of a context, a question, and an corresponding answer. We perform domain-specific fine-tuning on the pre-trained compressor using the SQuAD training set, followed by evaluation on SQuAD, HotpotQA [28], AdversarialQA [3], and Natural Questions (NQ) [15]. **Reference (w/o Context)** refers to generating responses using the downstream decoder conditioned solely on the question, without any additional context. **Reference (w/ Context)** denotes concatenating the un-compressed original context with the question as the input prompt.

For baseline methods, we maintain consistency with the settings in the PCC paper. To enable a direct and fair comparison, we utilize identical evaluation scripts and assess performance using F1 score and Exact Match (EM) metrics. The F1 score represents the harmonic mean of precision and recall, while the EM score indicates

whether the generated response is identical to the ground truth answer.

The results are presented in Table 2. On average, our method consistently surpasses both PCC-Lite and PCC-Large across all compression ratios. Notably, the performance advantage of our method becomes increasingly pronounced as the memory token budget decreases (e.g., at 16x and 64x compression). This empirical evidence strongly validates the efficiency of our sequential blocking strategy in maximizing information retention under constrained memory conditions.

4.2.2 In-Context Learning. Unlike RAG-based QA, which primarily demands precise evidence retrieval and local information extraction, In-Context Learning (ICL) necessitates the inference of latent patterns from demonstration examples and the subsequent application of these patterns to new queries via analogical reasoning. Given that RAG emphasizes local detail while ICL prioritizes global pattern recognition, we evaluate this capability separately.

We assess our method across three diverse datasets: GSM8K (grade school math word problems), SST-2 [26] (sentiment analysis), and WSC [16] (Winograd Schema Challenge for commonsense reasoning). For the ICL task, we fine-tune the pre-trained PIC checkpoint using the GSM8K training set. Our comparative analysis includes several baselines: zero-shot generation, few-shot ICL with maximum context limits of 150 and 750 tokens (uncompressed), and the PCC baseline utilizing 16x compressed in-context examples. To ensure a fair comparison, the PCC baseline employs the identical compressor architecture, training procedure, and downstream decoder as our PIC method.

The results are detailed in Table 3. On average, PIC not only surpasses the PCC baseline but also achieves optimal performance exceeding even the uncompressed few-shot baselines. Notably, our method exhibits a substantial advantage on the WSC dataset, indicating superior capability in retaining commonsense reasoning patterns within the compressed memory.

4.3 Block-wise Causal Mask Accelerates Compressor Learning

4.3.1 Pre-training Dynamics. We compare the pre-training loss trajectories to evaluate the learning efficiency of the compressor. As shown in Figure 5, our method exhibits a noticeably faster convergence rate during the initial phase of pre-training, achieving an acceleration of approximately 1.1 \times to 1.3 \times compared to the baseline. This empirically demonstrates that our approach, by explicitly constraining the receptive field to sequential blocks, effectively reduces the optimization complexity and facilitates the learning process for the compressor.

4.3.2 Data Efficiency Analysis. As observed in Figure 5, after 30k training steps, both PIC and the PCC baseline approach convergence, rendering it challenging to discern capability differences based solely on pre-training reconstruction loss. Consequently, to thoroughly investigate data efficiency, we perform domain-specific fine-tuning on checkpoints saved at various pre-training intervals

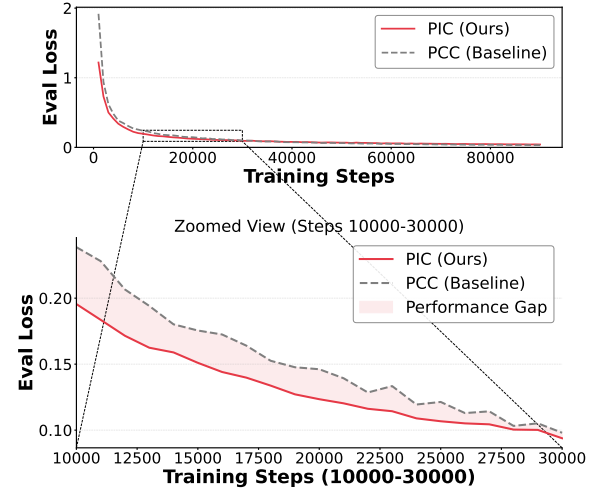


Figure 5: Comparison of Reconstruction Loss During Pre-training. The upper plot illustrates the overall loss trajectory, while the lower plot presents a zoomed-in view of steps 10k to 30k, highlighting the faster convergence of our PIC (red) compared to the PCC baseline (dashed gray).

and evaluate their performance on downstream QA tasks. To ensure a fair comparison with PCC, we utilize the identical Qwen2.5-0.5B-Instruct backbone for both methods, isolating the attention mechanism as the sole independent variable.

As demonstrated in Figure 6, our method achieves superior downstream performance compared to the PCC baseline using less than 1 billion pre-training tokens (Detailed results for other compression rates (4x and 64x) are shown in Figure 24 in Appendix D.). Remarkably, under the hardware setup of two 48GB RTX 4090 GPUs, our compressor requires only 56 hours of training to surpass the peak performance of the baseline, equivalent to a reduction in training time of approximately 40%. Furthermore, the performance of our method exhibits a consistent upward trend as the amount of pre-training data increases. In contrast, the PCC baseline fails to maintain a stable improvement with increased data, even showing performance degradation after 50k steps. These results collectively validate that our method significantly enhances both the data efficiency and training stability of the compressor.

4.4 Analysis of Learned Embeddings

Different from the claim by Louis et al. [20] that spatial specialization does not occur when the decoder is frozen, we hypothesize that such spatial specialization is, in fact, a critical indicator of effective compression. We calculated the cosine similarity between the memory embeddings generated by PIC and the original context token embeddings (For additional visualization results of spatial specialization across other datasets, please refer to Appendix B.2). As visualized in Figure 7, the learned attention patterns align perfectly with our imposed receptive field constraints: each memory token sequentially focuses intensively on the specific text chunk it is designated to compress.

Table 2: Comparative performance of various compression methods across four QA datasets. Bold values indicate the best performance for each dataset within the same compression ratio category, and second-best results are underlined. The values in parentheses denote the parameter size of the compressor used by each method.

Compression Rate	Methods	SQuAD		HotPotQA		AdversarialQA		NQ		Average	
		F_1	EM	F_1	EM	F_1	EM	F_1	EM	F_1	EM
1×	w/o Context	14.84	3.41	24.80	14.90	12.05	6.43	27.48	15.02	19.79	9.94
	w/ Context	79.81	59.97	64.60	51.12	56.10	38.67	64.64	51.38	66.29	50.29
40×	AutoCompressor	21.46	0.35	16.29	0.29	14.09	2.00	25.57	0.63	19.35	0.82
	xRAG	18.19	3.46	27.51	16.29	13.75	3.47	38.06	20.80	24.38	11.01
4×	ICAE (7B)	45.69	21.63	35.16	26.68	27.98	11.70	59.15	47.35	42.00	26.84
	LLMLingua2(0.6B)	51.20	32.18	55.72	<u>44.18</u>	35.41	24.80	68.44	55.85	52.69	39.25
	COCOM-Lite (0.1B)	21.70	9.17	40.07	32.32	19.45	13.90	50.45	41.87	32.92	24.32
	PCC-Lite (0.77B)	75.83	57.44	50.37	42.20	50.36	37.83	70.51	61.97	61.77	49.86
	PCC-Large (8B)	<u>77.76</u>	<u>60.04</u>	48.19	39.97	52.56	<u>39.37</u>	75.96	67.71	<u>63.62</u>	<u>51.77</u>
	OURS (PIC) (0.5B)	79.03	60.14	<u>54.66</u>	46.61	50.28	<u>38.13</u>	<u>71.82</u>	<u>62.47</u>	63.95	51.84
16×	COCOM-Lite (0.1B)	19.23	8.13	31.94	25.27	19.45	13.90	26.36	20.66	24.22	17.20
	PCC-Lite (0.77B)	56.82	37.72	35.67	27.88	40.94	<u>28.07</u>	62.56	52.73	49.00	36.60
	PCC-Large (8B)	55.32	37.72	33.76	25.27	38.96	26.47	71.09	61.97	49.78	37.86
	OURS (PIC) (0.5B)	59.41	39.86	41.05	<u>33.24</u>	39.98	27.73	67.61	58.37	<u>52.01</u>	<u>39.80</u>
	OURS (PIC) (1B)	<u>58.93</u>	<u>39.69</u>	<u>40.61</u>	<u>32.47</u>	<u>40.53</u>	29.00	<u>68.17</u>	<u>58.90</u>	52.06	40.02
64×	PCC-Lite (0.77B)	37.89	22.66	20.62	14.27	27.02	16.30	36.82	29.18	30.59	20.60
	OURS (PIC) (0.5B)	40.84	24.36	<u>30.54</u>	<u>23.07</u>	29.54	<u>19.40</u>	<u>57.96</u>	<u>49.15</u>	<u>39.72</u>	29.00

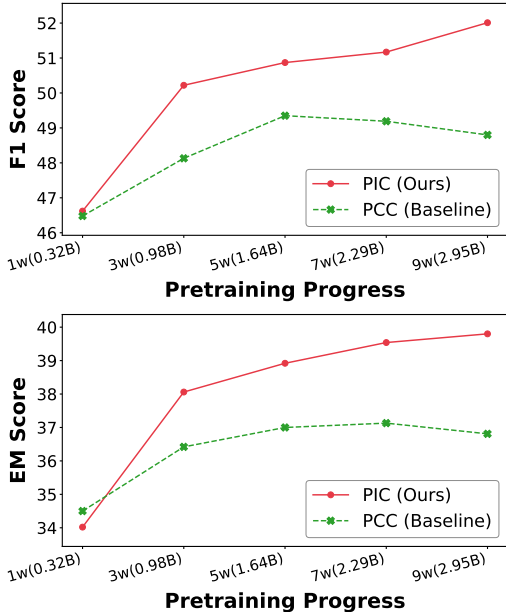


Figure 6: Relationship between Compressor Performance on Downstream QA Tasks and Pre-training Steps. The x-axis represents the number of tokens corresponding to the pre-training steps (converted to 1 epoch equivalent), and the y-axis represents the EM or F1 score.

Table 3: Performance Comparison on Three ICL Datasets (Accuracy %). "Comp." denotes using compressed memory context. Bold indicates the highest accuracy.

Methods	GSM8K	SST-2	WSC	Average
Zero-shot	77.81	90.57	57.69	75.36
ICL 150 Tokens	83.56	95.41	50.00	76.32
ICL 750 Tokens	86.10	94.95	46.15	75.73
PCC-16x Comp. 150 Tokens	90.11	92.09	43.27	75.16
PCC-16x Comp. 750 Tokens	91.44	90.02	47.12	76.19
OURS (16x Comp. 150 Tokens)	89.84	88.65	57.69	78.73
OURS (16x Comp. 750 Tokens)	90.64	87.61	65.38	81.21

Furthermore, we investigated the internal coherence of the memory slots by analyzing the pairwise cosine similarity between memory tokens (m_i, m_j) (We also conducted this analysis on other datasets; for detailed results, please refer to Appendix C). As illustrated in Figure 8, the memory embeddings generated by the PCC exhibit a problematic distribution. Specifically, The PCC distribution displays a heavy right tail, indicating high similarity and redundancy among certain memory embeddings. Conversely, the presence of negative cosine similarities on the left side suggests potential adversarial semantics between some memory tokens. Most notably, the distribution exhibits a bimodal characteristic; the left peak, most memory embeddings have similarities between 0 and

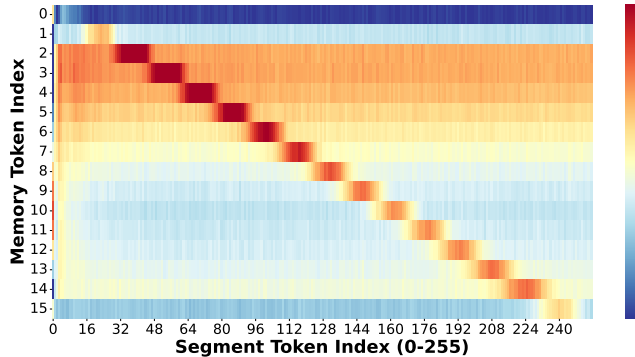


Figure 7: Heatmap visualization of the cosine similarity between memory embeddings (PIC) generated by the Fully Trained Compressor (90k Steps) and original token embeddings on the HotpotQA dataset. Red indicates higher similarity, while blue represents lower similarity.

Table 4: Ablation Study: Average performance across four datasets in the RAG-based QA domain. Reported metrics are in percentage (%).

Method	F1	EM
16x-PIC	52.01	39.80
Full Causal Mask (16x-PCC)	48.80	36.81

0.2, implying that a portion of the memory embeddings may serve as redundant noise.

In contrast, our PIC method yields a distribution that approximates a normal distribution, significantly mitigating potential adversarial semantics, low-similarity noise and the high-similarity redundancy. This statistical evidence suggests that our block-wise approach facilitates the learning of more distinct, orthogonal, and information-rich representations for each memory token.

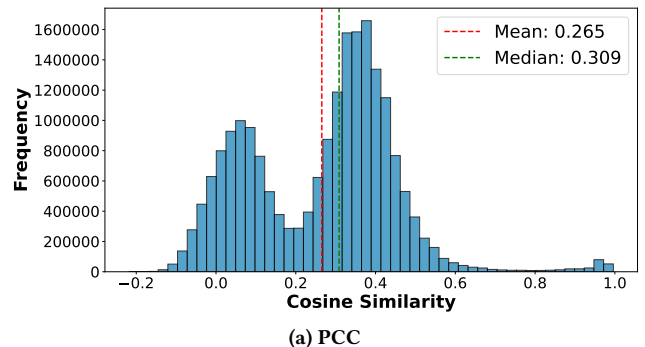
4.5 Ablation Study

To strictly isolate the effectiveness of our proposed block-wise causal mask, we conducted an ablation study at a $16\times$ compression ratio. We utilized the representative Qwen2.5-0.5B-Instruct backbone for all variants to factor out potential performance gaps caused by different model architectures, strictly varying only the attention mask configuration. The baseline configuration, denoted as Full Causal Mask, retains the standard global causal attention mechanism utilized in the original PCC framework.

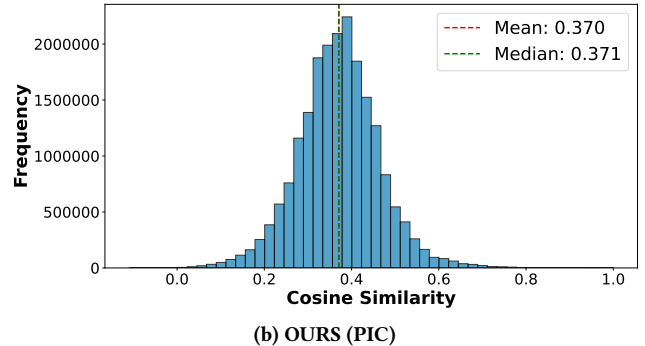
As shown in Table 4 (for the complete table, please refer to Table 5 in the Appendix), our method significantly outperforms the Full Causal Mask baseline. This comparison confirms that the observed performance gains are directly due to our proposed masking strategy rather than the choice of the compressor backbone.

5 Conclusion

Drawing inspiration from the chunking mechanism in human working memory and the observed spatial specialization of memory



(a) PCC



(b) OURS (PIC)

Figure 8: Distribution of pairwise cosine similarities between memory embeddings within the same memory slot on the HotpotQA dataset. Compressors are fine-tuned on downstream QA tasks.

embeddings relative to original tokens, we introduced Parallelized Iterative Compression (PIC). By implementing a straightforward modification to the Transformer attention mask, PIC explicitly constrains the receptive field of memory tokens to sequential local blocks. This structural inductive bias significantly reduces the optimization complexity inherent in compressor training. Empirical results across multiple downstream tasks demonstrate that our method outperforms a wide range of competitive baselines. This advantage is particularly pronounced in high-compression scenarios; for example, with a compression ratio of $64\times$, PIC achieves relative improvements of 29.8% in F1 score and 40.7% in EM score on QA tasks. Furthermore, our approach substantially accelerates the training process. Specifically, for the $16\times$ compressor, our method surpasses the baseline’s peak performance with approximately 40% less training time, demonstrating significantly improved data efficiency. We also observed that extending training with additional data yields continuous performance gains. Finally, we shed light on the intrinsic properties of text embeddings, suggesting that the phenomenon of spatial specialization may serve as a critical indicator of compressor efficacy. We hope these findings will offer valuable insights to inspire future research in the field of context compression.

References

- [1] Alan Baddeley. 1992. Working Memory. *Science* 255, 5044 (1992), 556.
- [2] Omri Barak and Misha Tsodyks. 2014. Working models of working memory. *Current opinion in neurobiology* 25 (2014), 20–24.

[3] Max Bartolo, Alastair Roberts, Johannes Welbl, Sebastian Riedel, and Pontus Stenetorp. 2020. Beat the AI: Investigating adversarial human annotation for reading comprehension. *Transactions of the Association for Computational Linguistics* 8 (2020), 662–678.

[4] Xin Cheng, Xun Wang, Xingxing Zhang, Tao Ge, Si-Qing Chen, Furu Wei, Huishuai Zhang, and Dongyan Zhao. 2024. xrag: Extreme context compression for retrieval-augmented generation with one token. *Advances in Neural Information Processing Systems* 37 (2024), 109487–109516.

[5] Alexis Chevalier, Alexander Wettig, Anirudh Ajith, and Danqi Chen. 2023. Adapting Language Models to Compress Contexts. In *Proceedings of the 2023 Conference on Empirical Methods in Natural Language Processing*. Association for Computational Linguistics.

[6] Yu Neng Chuang, Tianwei Xing, Chia Yuan Chang, Zirui Liu, Xun Chen, and Xia Hu. 2024. Learning to Compress Prompt in Natural Language Formats. In *2024 Conference of the North American Chapter of the Association for Computational Linguistics: Human Language Technologies, NAACL 2024*. Association for Computational Linguistics (ACL), 7749–7760.

[7] Karl Cobbe, Vineet Kosaraju, Mohammad Bavarian, Mark Chen, Heewoo Jun, Lukasz Kaiser, Matthias Plappert, Jerry Tworek, Jacob Hilton, Reichiro Nakano, et al. 2021. Training verifiers to solve math word problems. *arXiv preprint arXiv:2110.14168* (2021).

[8] Nelson Cowan. 2010. The magical mystery four: How is working memory capacity limited, and why? *Current directions in psychological science* 19, 1 (2010), 51–57.

[9] Yuhong Dai, Jianxun Lian, Yitian Huang, Wei Zhang, Mingyang Zhou, Mingqi Wu, Xing Xie, and Hao Liao. 2025. Pretraining context compressor for large language models with embedding-based memory. In *Proceedings of the 63rd Annual Meeting of the Association for Computational Linguistics (Volume 1: Long Papers)*, 28715–28732.

[10] Yunfan Gao, Yun Xiong, Xinyu Gao, Kangxiang Jia, Jinliu Pan, Yuxi Bi, Yixin Dai, Jiawei Sun, Haofen Wang, and Haofen Wang. 2023. Retrieval-augmented generation for large language models: A survey. *arXiv preprint arXiv:2312.10997* 2, 1 (2023).

[11] Tao Ge, Hu Jing, Lei Wang, Xun Wang, Si-Qing Chen, and Furu Wei. 2024. In-context Autoencoder for Context Compression in a Large Language Model. In *The Twelfth International Conference on Learning Representations*. <https://openreview.net/forum?id=uREj4ZuGJE>

[12] Anirudh Goyal and Yoshua Bengio. 2022. Inductive biases for deep learning of higher-level cognition. *Proceedings of the Royal Society A* 478, 2266 (2022), 20210068.

[13] Huiqiang Jiang, Qianhui Wu, Chin-Yew Lin, Yuqing Yang, and Lili Qiu. 2023. LLMlingua: Compressing Prompts for Accelerated Inference of Large Language Models. In *Proceedings of the 2023 Conference on Empirical Methods in Natural Language Processing*, 13358–13376.

[14] Huiqiang Jiang, Qianhui Wu, Xufang Luo, Dongsheng Li, Chin-Yew Lin, Yuqing Yang, and Lili Qiu. 2024. Longllmllingua: Accelerating and enhancing llms in long context scenarios via prompt compression. In *Proceedings of the 62nd Annual Meeting of the Association for Computational Linguistics (Volume 1: Long Papers)*, 1658–1677.

[15] Vladimir Karpukhin, Barlas Onguz, Sewon Min, Patrick SH Lewis, Ledell Wu, Sergey Edunov, Danqi Chen, and Wen-tau Yih. 2020. Dense Passage Retrieval for Open-Domain Question Answering.. In *EMNLP (1)*, 6769–6781.

[16] Hector J Levesque, Ernest Davis, and Leora Morgenstern. 2012. The Winograd schema challenge. *KR 2012*, 13th (2012), 3.

[17] Tianle Li, Ge Zhang, Quy Duc Do, Xiang Yue, and Wenhui Chen. 2024. Long-context llms struggle with long in-context learning. *arXiv preprint arXiv:2404.02060* (2024).

[18] Yuchen Li, Bi Dong, Frank Guerin, and Chenghua Lin. 2023. Compressing context to enhance inference efficiency of large language models. In *Proceedings of the 2023 conference on empirical methods in natural language processing*, 6342–6353.

[19] Zongqian Li, Yinhong Liu, Yixuan Su, and Nigel Collier. 2025. Prompt compression for large language models: A survey. In *Proceedings of the 2025 Conference of the Nations of the Americas Chapter of the Association for Computational Linguistics: Human Language Technologies (Volume 1: Long Papers)*, 7182–7195.

[20] Maxime Louis, Hervé Déjean, and Stéphane Clinchant. 2025. PISCO: Pretty Simple Compression for Retrieval-Augmented Generation. In *Findings of the Association for Computational Linguistics: ACL 2025*. Wanxiang Che, Joyce Nabende, Ekataterina Shutova, and Mohammad Taher Pilehvar (Eds.). Association for Computational Linguistics, Vienna, Austria, 15506–15521. [doi:10.18653/v1/2025.findings-acl.800](https://doi.org/10.18653/v1/2025.findings-acl.800)

[21] Jesse Mu, Xiang Li, and Noah Goodman. 2023. Learning to compress prompts with gist tokens. *Advances in Neural Information Processing Systems* 36 (2023), 19327–19352.

[22] Zhuoshi Pan, Qianhui Wu, Huiqiang Jiang, Menglin Xia, Xufang Luo, Jue Zhang, Qingwei Lin, Victor Röhle, Yuqing Yang, Chin-Yew Lin, et al. 2024. LLMlingua-2: Data Distillation for Efficient and Faithful Task-Agnostic Prompt Compression. In *Findings of the Association for Computational Linguistics ACL 2024*, 963–981.

[23] Guilherme Penedo, Hynek Kydlicek, Anton Lozhkov, Margaret Mitchell, Colin A Raffel, Leandro Von Werra, Thomas Wolf, et al. 2024. The fineweb datasets: Decanting the web for the finest text data at scale. *Advances in Neural Information Processing Systems* 37 (2024), 30811–30849.

[24] Pranav Rajpurkar, Robin Jia, and Percy Liang. 2018. Know What You Don’t Know: Unanswerable Questions for SQuAD. In *Proceedings of the 56th Annual Meeting of the Association for Computational Linguistics (Volume 2: Short Papers)*, 784–789.

[25] David Rau, Shuai Wang, Hervé Déjean, Stéphane Clinchant, and Jaap Kamps. 2025. Context Embeddings for Efficient Answer Generation in Retrieval-Augmented Generation. In *Proceedings of the Eighteenth ACM International Conference on Web Search and Data Mining (Hannover, Germany) (WSDM ’25)*. Association for Computing Machinery, New York, NY, USA, 493–502. [doi:10.1145/3701551.3703527](https://doi.org/10.1145/3701551.3703527)

[26] Richard Socher, Alex Perelygin, Jean Wu, Jason Chuang, Christopher D Manning, Andrew Y Ng, and Christopher Potts. 2013. Recursive deep models for semantic compositionality over a sentiment treebank. In *Proceedings of the 2013 conference on empirical methods in natural language processing*, 1631–1642.

[27] Baosong Yang, Zhaopeng Tu, Derek F Wong, Fandong Meng, Lidia S Chao, and Tong Zhang. 2018. Modeling Localness for Self-Attention Networks. In *Proceedings of the 2018 Conference on Empirical Methods in Natural Language Processing*, 4449–4458.

[28] Zhihui Yang, Peng Qi, Saizheng Zhang, Yoshua Bengio, William Cohen, Ruslan Salakhutdinov, and Christopher D Manning. 2018. HotpotQA: A dataset for diverse, explainable multi-hop question answering. In *Proceedings of the 2018 conference on empirical methods in natural language processing*, 2369–2380.

[29] Weishun Zhong, Mikhail Katkov, and Misha Tsvydkys. 2024. Synaptic Theory of Chunking in Working Memory. *arXiv preprint arXiv:2408.07637* (2024).

A Heatmap Visualization of Spatial Specialization Phenomena in ICAE

We also conducted a cosine similarity analysis between memory embeddings and original token embeddings on ICAE. The number of memory tokens in the fixed memory slots of ICAE is set to 128. We analyzed texts with a length of 512. As shown in Figure 9, the image appears chaotic, and no obvious spatial specialization phenomenon was observed.

B Heatmap Visualization of Spatial Specialization Phenomena on Other Datasets

B.1 PCC

We similarly conducted visualization experiments on the spatial specialization phenomenon of PCC across other datasets, as shown in Figure 10, Figure 11, Figure 12, Figure 13, Figure 14, Figure 15 and Figure 16, we observe that this spatial specialization phenomenon is dataset-independent, with texts across different datasets exhibiting consistent spatial specialization patterns. Furthermore, the features become more pronounced as the number of samples in the dataset increases. However, in the case of the AdversarialQA dataset, the statistical regularity is less evident. This is primarily because the samples are generally short, with the majority having a length of less than 256 tokens.

B.2 OURS (PIC)

We similarly conducted visualization experiments on the spatial specialization phenomenon of our method across other datasets, as shown in Figure 17, Figure 18, Figure 19, and Figure 20, PIC displays a sharp and consistent diagonal pattern across all evaluated domains. This confirms that our block-wise causal mask effectively enforces the intended receptive field constraints, ensuring that each memory token is exclusively dedicated to compressing its corresponding local context chunk. This structural alignment is robust

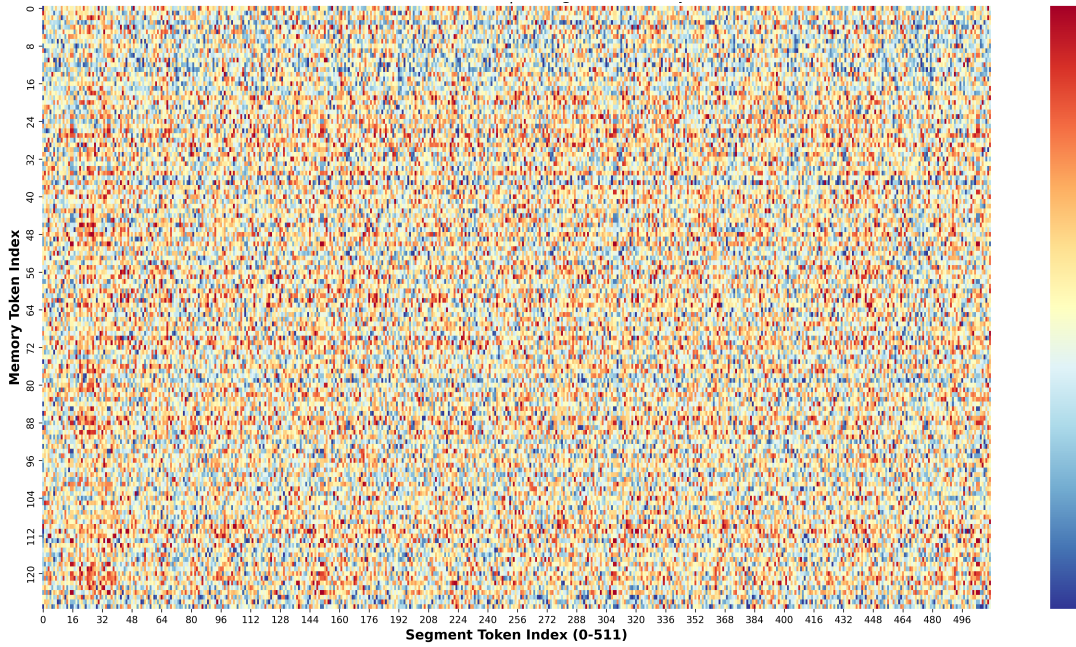
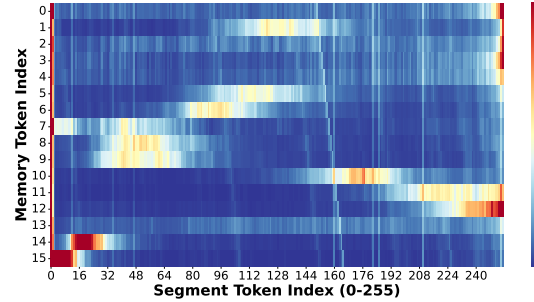
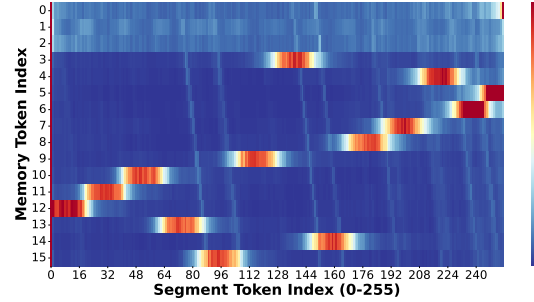


Figure 9: Heatmap visualization of the cosine similarity between memory embeddings (PCC) and original token embeddings on the SQuAD dataset. Red indicates higher similarity, while blue represents lower similarity.



(a) pre-trained compressor



(b) fine-tuned compressor

Figure 10: Attention weight heatmap between memory tokens and original context tokens on the SQuAD dataset.

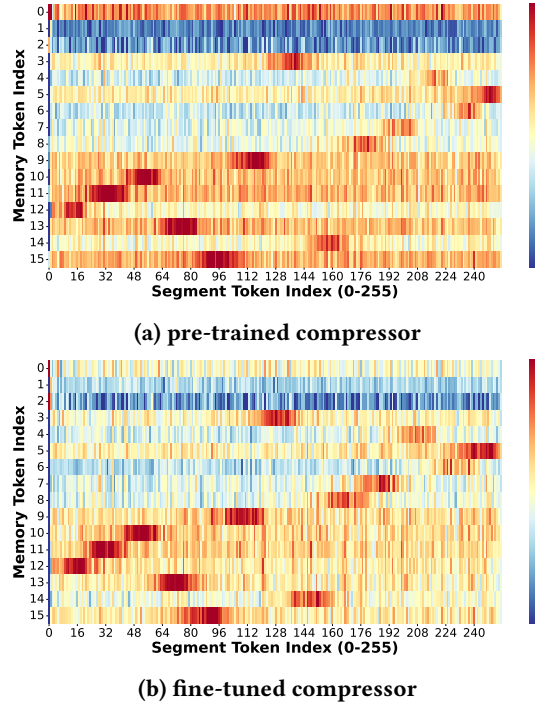


Figure 11: Heatmap visualization of the cosine similarity between memory embeddings (PCC) and original token embeddings on the SQuAD dataset. Red indicates higher similarity, while blue represents lower similarity.

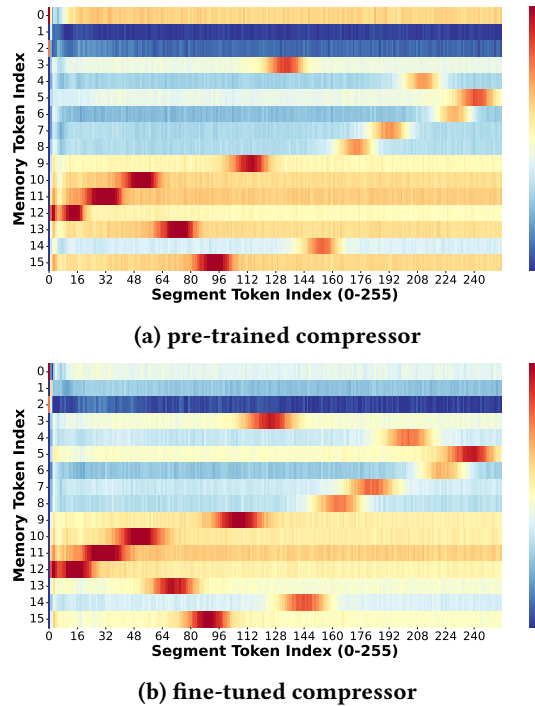
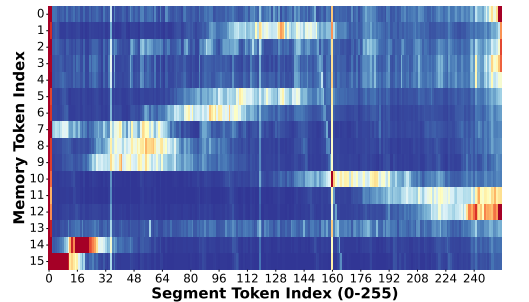
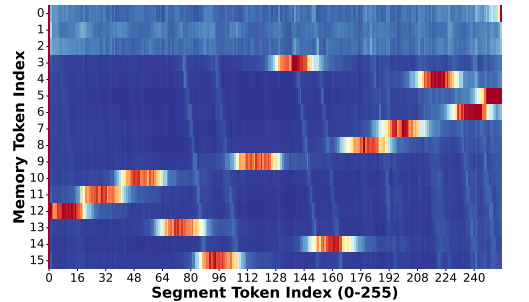


Figure 12: Heatmap visualization of the cosine similarity between memory embeddings (PCC) and original token embeddings on the HotpotQA dataset. Red indicates higher similarity, while blue represents lower similarity.

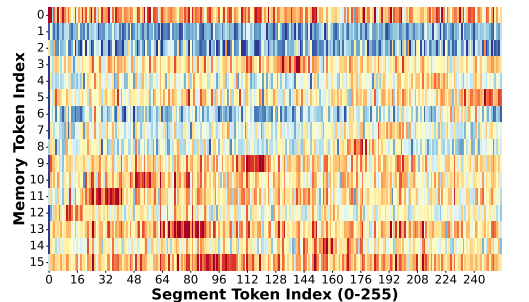


(a) pre-trained compressor

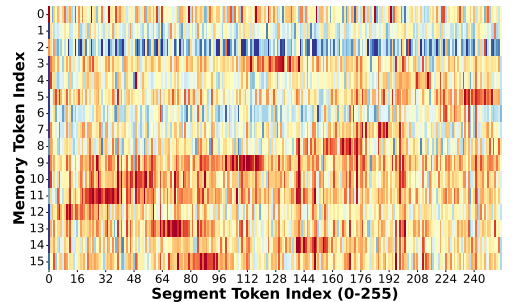


(b) fine-tuned compressor

Figure 13: Attention weight heatmap between memory tokens and original context tokens on the AdversarialQA dataset.



(a) pre-trained compressor



(b) fine-tuned compressor

Figure 14: Heatmap visualization of the cosine similarity between memory embeddings (PCC) and original token embeddings on the AdversarialQA dataset. Red indicates higher similarity, while blue represents lower similarity.

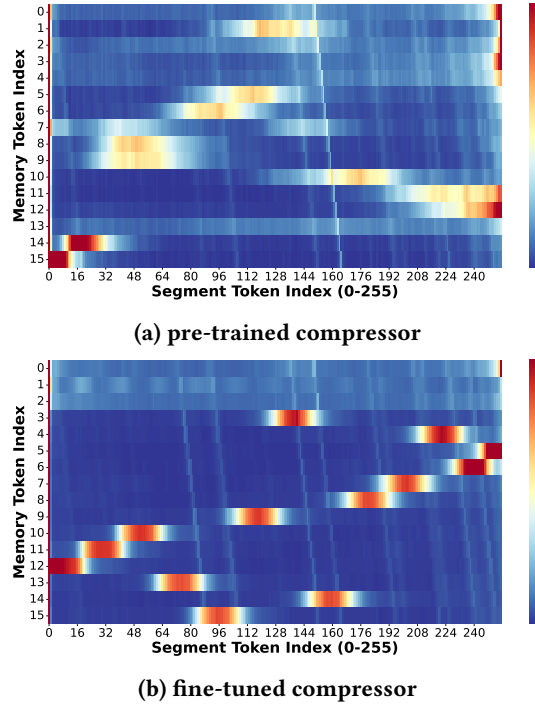


Figure 15: Attention weight heatmap between memory tokens and original context tokens on the Natural Questions dataset.

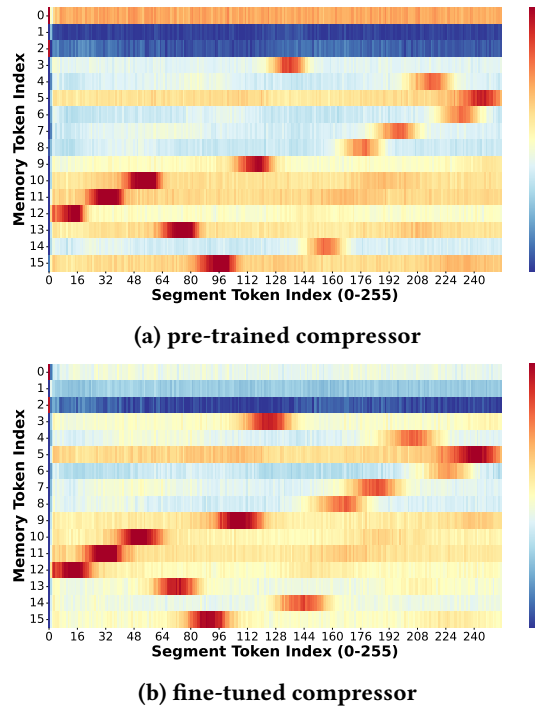


Figure 16: Heatmap visualization of the cosine similarity between memory embeddings (PCC) and original token embeddings on the Natural Questions dataset. Red indicates higher similarity, while blue represents lower similarity.

across different data distributions, validating the generalizability of our approach..

C Analysis of Cosine Similarity Between Embedding Pairs on Other Datasets

We also analyzed the cosine similarity between memory embeddings on other datasets; see Figure 21, Figure 22, and Figure 23, the pairwise cosine similarity distributions for PCC consistently exhibit a bimodal pattern with a heavy tail of high similarity, indicating significant redundancy and potential mode collapse among memory tokens. Conversely, PIC maintains a distribution centered around zero with lower variance across all datasets. This suggests that our method produces more orthogonal and information-dense memory representations, effectively utilizing the memory budget by minimizing inter-token redundancy..

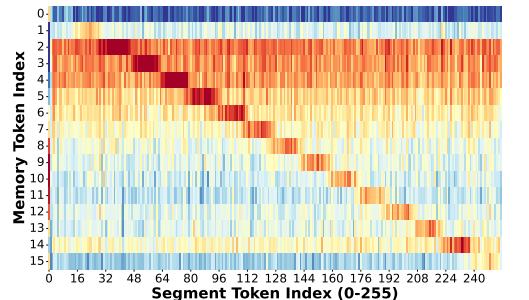
D Data Efficiency Analysis on Other Compression Rate

We further investigated the data efficiency of our method under different compression regimes. Figure 24 presents the performance

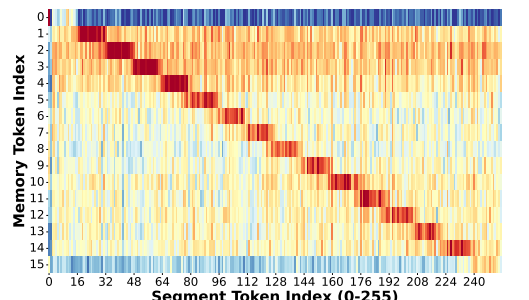
trajectories for 4x and 64x compression rates. Consistent with the 16x results discussed in the main text, PIC demonstrates a superior learning curve. For both compression ratios, our method achieves higher downstream performance (EM and F1 scores) at earlier pre-training steps compared to the baseline, confirming that the block-wise constraint accelerates the acquisition of effective compression capabilities regardless of the compression granularity.

E Complete Results of Ablation Study

Table 5 provides the comprehensive breakdown of our ablation study. Across all four datasets (SQuAD, HotPotQA, AdversarialQA, and NQ), the PIC model equipped with the block-wise causal mask consistently outperforms the variant using a full causal mask (PCC setting). The performance gap is evident in both F1 and EM metrics, statistically validating that the structured inductive bias introduced by our masking strategy is the primary driver of the observed improvements, rather than the model architecture alone.

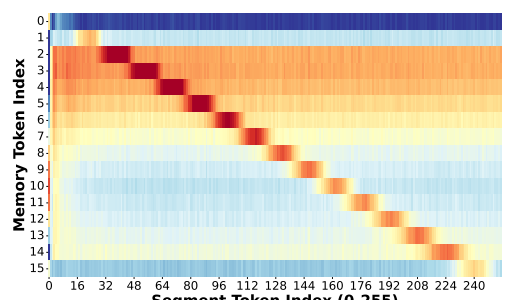


(a) pre-trained compressor

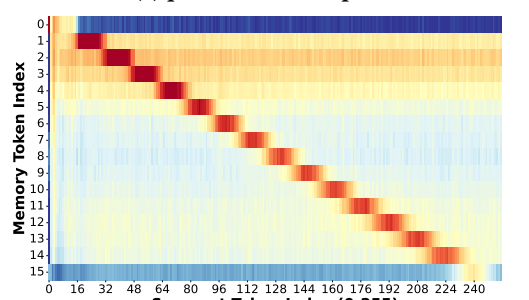


(b) fine-tuned compressor

Figure 17: Heatmap visualization of the cosine similarity between memory embeddings (PIC) and original token embeddings on the SQuAD dataset. Red indicates higher similarity, while blue represents lower similarity.

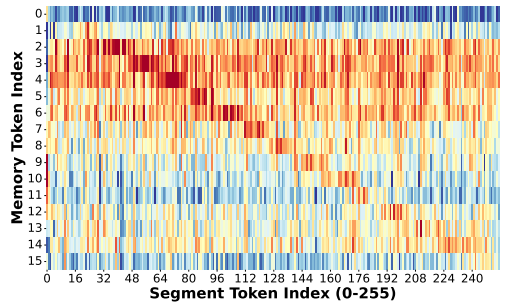


(a) pre-trained compressor

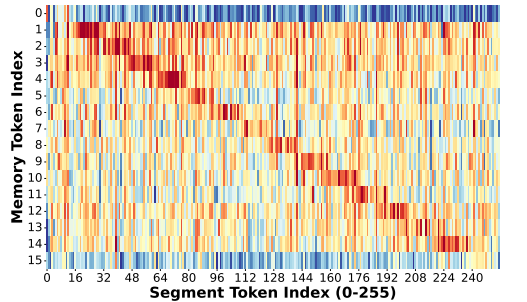


(b) fine-tuned compressor

Figure 18: Heatmap visualization of the cosine similarity between memory embeddings (PIC) and original token embeddings on the HotpotQA dataset. Red indicates higher similarity, while blue represents lower similarity.

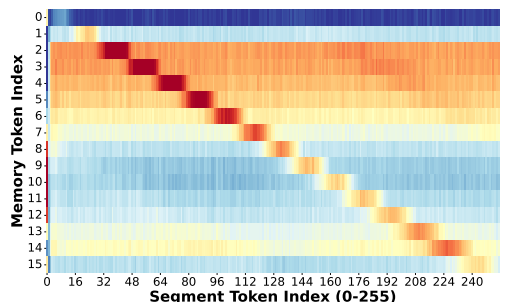


(a) pre-trained compressor

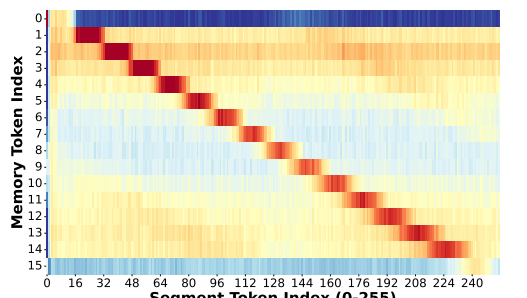


(b) fine-tuned compressor

Figure 19: Heatmap visualization of the cosine similarity between memory embeddings (PIC) and original token embeddings on the AdversarialQA dataset. Red indicates higher similarity, while blue represents lower similarity.

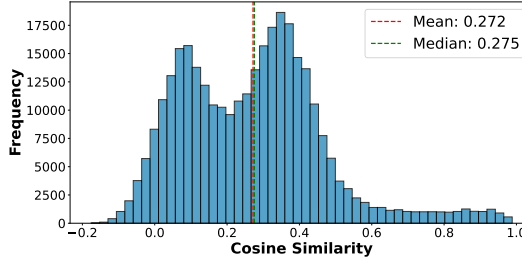


(a) pre-trained compressor

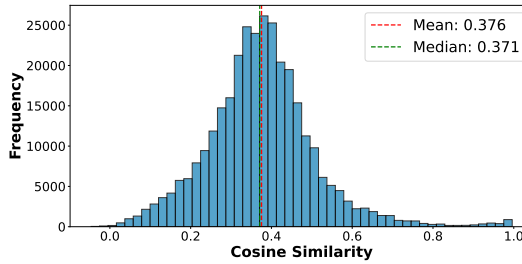


(b) fine-tuned compressor

Figure 20: Heatmap visualization of the cosine similarity between memory embeddings (PIC) and original token embeddings on the Natural Questions dataset. Red indicates higher similarity, while blue represents lower similarity.

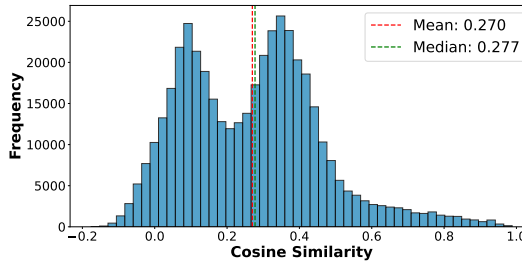


(a) PCC

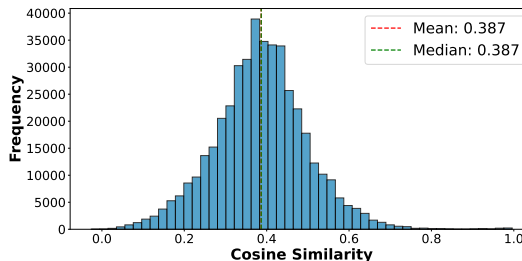


(b) OURS (PIC)

Figure 21: Visualization of pairwise cosine similarity distributions between memory embeddings within the same memory slot on the SQuAD dataset. The compressors used are fine-tuned on downstream QA tasks.



(a) PCC



(b) OURS (PIC)

Figure 22: Visualization of pairwise cosine similarity distributions between memory embeddings within the same memory slot on the AdversarialQA dataset. The compressors used are fine-tuned on downstream QA tasks.

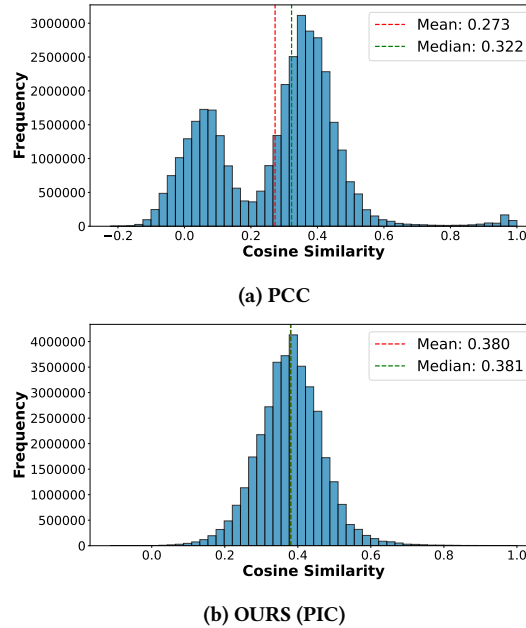


Figure 23: Visualization of pairwise cosine similarity distributions between memory embeddings within the same memory slot on the Natural Questions dataset. The compressors used are fine-tuned on downstream QA tasks.

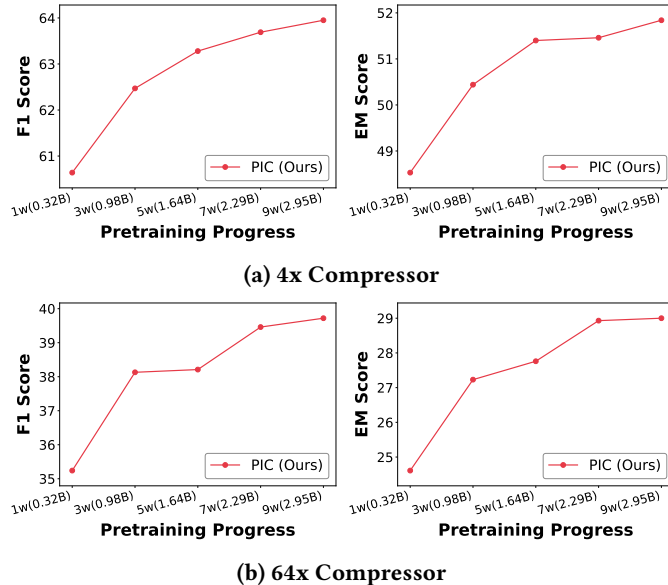


Figure 24: Relationship between Compressor Performance on Downstream QA Tasks and Pre-training Steps. The x-axis represents the number of tokens corresponding to the pre-training steps (converted to 1 epoch equivalent), and the y-axis represents the EM or F1 score.

Table 5: Ablation Study: The table presents the performance (F1 and Exact Match (EM)) across four datasets: SQuAD, HotPotQA, AdversarialQA, and NQ, along with the average metrics. Our method is compared with the PCC baseline (using full causal mask). Best-performing results for each dataset are highlighted in bold.

Methods	SQuAD		HotPotQA		AdversarialQA		NQ		Average	
	F_1	EM	F_1	EM	F_1	EM	F_1	EM	F_1	EM
OURS (PIC)	59.41	39.86	41.05	33.24	39.98	27.73	67.61	58.37	52.01	39.80
w/ full causal mask (PCC)	55.37	36.12	36.07	28.24	37.16	24.93	66.60	57.93	48.80	36.81